materials

MDPI

Article

Effect of Mineral Admixtures on Physical, Mechanical, and Microstructural Properties of Flue Gas Desulfurization Gypsum-Based Self-Leveling Mortar

Shiyu Wang, Yanxin Chen *, Wei Zhao and Chang Chen *

College of Materials Science and Engineering, Xi'an University of Architecture & Technology, Xi'an 710055, China; wangshiyu@xauat.edu.cn (S.W.); zhaowei@xauat.edu.cn (W.Z.)

* Correspondence: chen_yanxin@xauat.edu.cn (Y.C.); changchen420@xauat.edu.cn (C.C.); Tel.: +86-130-9697-3109 (Y.C.)

Abstract: The production of flue gas desulfurization gypsum poses a serious threat to the environment. Thus, utilizing gypsum-based self-leveling mortar (GSLM) stands out as a promising and effective approach to address the issue. β-hemihydrate gypsum, cement, polycarboxylate superplasticizer, hydroxypropyl methyl cellulose ether (HPMC), retarder, and defoamer were used to prepare GSLM. The impact of mineral admixtures (steel slag (SS), silica fume (SF), and fly ash (FA)) on the physical, mechanical, and microstructural properties of GSLM was examined through hydration heat, X-ray diffractometry (XRD), Raman spectroscopy, and scanning electron microscopy (SEM) analyses. The GSLM benchmark mix ratio was determined as follows: 94% of desulfurization building gypsum, 6% of cement, 0.638% each of water reducer and retarder, 0.085% each of HPMC and defoamer (calculated additive ratio relative to gypsum), and 0.54 water-to-cement ratio. Although the initial fluidity decreased in the GSLM slurry with silica fume, there was minimal change in 30 min fluidity. Notably, at an SS content of 16%, the GSLM exhibited optimal flexural strength (6.6 MPa) and compressive strength (20.4 MPa). Hydration heat, XRD, and Raman analyses revealed that a small portion of SS actively participated in the hydration reaction, while the remaining SS served as a filler.

Keywords: flue gas desulfurization gypsum-based self-leveling mortar; steel slag; silica fume; fly ash; properties

check for updates

Citation: Wang, S.; Chen, Y.; Zhao, W.; Chen, C. Effect of Mineral Admixtures on Physical, Mechanical, and Microstructural Properties of Flue Gas Desulfurization Gypsum-Based Self-Leveling Mortar. *Materials* **2024**, *17*, 2227. https://doi.org/10.3390/ma17102227

Academic Editor: Lucjan Chmielarz

Received: 26 March 2024
Revised: 26 April 2024
Accepted: 6 May 2024
Published: 9 May 2024

Copyright: © 2024 by the authors. Licensee MDPI, Basel, Switzerland. This article is an open access article distributed under the terms and conditions of the Creative Commons Attribution (CC BY) license (https://creativecommons.org/licenses/by/4.0/).

1. Introduction

In recent years, the global production of flue gas desulfurization gypsum (FGDG) has surged, with annual emissions exceeding 255 million tons [1]. Currently, with the continuous increase in energy consumption and increasingly stringent environmental requirements, the production of FGDG in China has exceeded 100 million tons [2]. The prolonged and extensive storage of FGDG not only consumes land resources, but the gypsum also contains impurities that seriously pollute the environment through water, air, and soil contamination [3,4]. Currently, FGDG is primarily utilized in the realm of building materials [5–11]. The use of FGDG for the remediation of phosphorous leaching in soil plants could be advantageous to improve agriculture land harvesting yields [12].

Within the domain of building construction, essential projects include the laying and backfilling of underfloor heating, as well as the leveling of floors, creating a substantial demand for self-leveling materials. Nevertheless, traditional cement-based self-leveling mortar has disadvantages such as poor thermal conductivity and low construction efficiency [13]. Gypsum, with its early strength and minimal shrinkage, proves advantageous, prompting its substitution for cement in the preparation of self-leveling materials. Canbaz et al. [14] studied the impact of various fine aggregates and water-reducing agents on the performance of gypsum-based self-leveling mortar (GSLM). The GSLM

demonstrated 28-day compressive strength, shear strength, and water absorption rate of 34 MPa, 4.6 MPa, and 1.3%, respectively.

GSLMs are widely employed as fillers for floor heating systems, known for their excellent leveling performance, rapid solidification, high early strength, and versatility [15–21]. However, gypsum, the main component, demands a significant amount of water, leading to compromised strength in the later stages. To enhance its performance, additional materials must be incorporated. Furthermore, the need for additives to meet fluidity and setting time requirements is crucial. However, impurities in FGDG can impact additive effectiveness, limiting practical engineering use [22–24]. Yang [25] and Zhang [26] delved into the effect of gypsum on cement-based self-leveling mortar, highlighting its role as both a filler and a participant in hydration. Xiao et al. [27] utilized β-hemihydrate gypsum and sulfoaluminate cement in GSLM preparation, resulting in a well-connected structure and robust mechanical properties for products derived from desulfurization building gypsum.

The introduction of fillers or additives can enhance GSLM performance. Zhang et al. [28] explored the impact of aggregates on GSLM physical properties, revealing that molybdenum tailings with <45% content can serve as suitable aggregates. External additives exhibit interactive effects, with polycarboxylate-based, high-efficiency, water-reducing agents proving adept at dispersing gypsum particles [29,30].

Scholars have extensively researched the reinforcing effect of mineral admixtures on composite materials. Li et al. [31] added cement, fly ash, and lime to gypsum and observed that the compressive strength increased when the ratio of cement, fly ash, and lime was 10%, 20%, and 14.86%, respectively. Guo et al. [32] determined that a 75% desulfurization gypsum, 5% cement, and 20% mineral powder ratio yielded FGDG blocks with good physical properties. Zhou et al. [33] discovered that stone-based composite materials exhibited robust mechanical properties when aluminate cement, mineral powder, and quicklime were added to building desulfurization gypsum. However, research on mineral admixture application in self-leveling systems is limited, and mechanistic exploration is lacking.

This study employed FGDG and ordinary Portland cement as primary cementitious materials to formulate GSLM. The influence of steel slag (SS), silica fume (SF), and fly ash (FA) as mineral admixtures on the physical, mechanical, and microscopic properties of GSLM was systematically investigated, leading to the determination of optimal mineral admixture proportions. The use of various mineral admixtures effectively improves the performance of gypsum-based self-leveling mortar while significantly reducing the production cost of the material, resulting in the resourceful utilization of multiple solid wastes.

2. Materials and Methods

2.1. Materials

Ordinary Portland cement (Grade 42.5R) was procured from Wuxi Tianshan Cement Co., Ltd. (Wuxi, China) FGDG ($CaSO_4 \cdot 2H_2O$) was obtained from Datang Power Plant (Henan, China). Its initial and final setting times were 168 and 202 min respectively, 3-day and 28-day flexural strength was 6.2 and 9.3 MPa, 3-day and 28-day compressive strength was 36.2 and 62.3 MPa, respectively. Desulfurization building gypsum underwent production at 170–190 °C, followed by aging before use. The performance characteristics of desulfurization building gypsum are detailed in Table 1 and Figure 1. As shown in the figure, the main mineral phases of desulfurization building gypsum are hemihydrate gypsum and a small amount of anhydrous gypsum. The chemical composition is shown in Table 2. Polycarboxylate superplasticizer (bulk density 500–700 g/L, containing active ingredients > 90%) can reduce the water required for mixing without reducing fluidity, Hydroxypropyl methyl cellulose ether (HPMC, active ingredient content $\geq$ 90%, pH 6–8) can enhance the water retention performance of mortar and prevent mortar bleeding. Polymeric amino acid retarder (bulk density 640 $\pm$ 50 g/L, fineness $\leq$ 300 μm) can prolong the hydration time of desulfurization gypsum, and defoamer powder polyether (pH 6–8)

can reduce air bubbles in mortar. Four types of additives were sourced from Jiangsu Zhaojia Building Materials Technology Co., Ltd. (Jiangsu, China).

Table 1. Composition and performance of desulfurization building gypsum.

Project	Numerical Value
Anhydrite (%)	15.98
Hemihydrate gypsum (%)	84.02
Dihydrate gypsum (%)	0.00
Setting time (min)	3
2-h compressive strength (MPa)	4.06
2-h flexural strength (MPa)	2.26
Requirement of normal consistency (g/100 g)	85

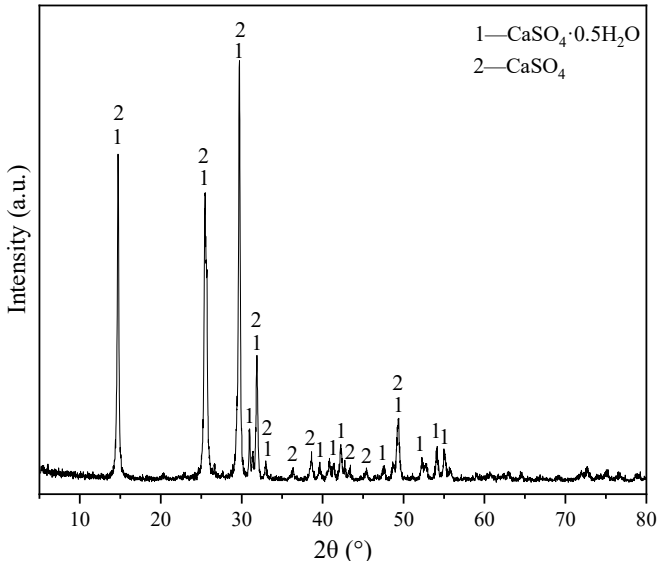


Figure 1. XRD spectrum of desulfurization building gypsum.

Table 2. Chemical compositions of the raw materials (%).

Compositions	Na_2O	MgO	Al_2O_3	SiO_2	SO_3	CaO	TiO_2	K_2O	MnO	Fe_2O_3	Other
Gypsum	-	0.81	1.07	1.97	54.10	40.60	-	0.20	-	0.44	0.81
Cement (OPC)	-	0.64	4.21	18.59	4.22	65.95	0.23	-	-	2.95	3.21
Steel slag	0.27	7.78	4.39	15.30	0.38	39.20	1.39	-	4.93	22.70	3.66
Silica fume	-	1.34	0.12	45.43	0.05	52.63	-	0.03	0.02	0.22	0.16
Fly ash	1.07	1.19	24.30	50.60	1.52	8.50	1.27	2.16	-	8.60	0.79

The chemical compositions of the three mineral admixtures—SS, SF, and FA—are presented in Table 2. SS primarily consists of CaO, SiO_2, and Fe_2O_3, with an average particle size of 9.34 μm. According to the requirements of GB/T 20491-2017, "Steel slag powder used for cement and concrete", the activity index of steel slag was tested, and its strength activity indexes at 7 and 28 days were 78.3% and 83.1%, respectively. SF is primarily composed of SiO_2 and CaO with an average particle size of 1.45 μm. According to the requirements of GB/T 27690-2023. "Silica fume for cement mortar and concrete", the activity index of silica fume was tested, and its strength activity index at 7 days was 70%. FA is primarily composed of SiO_2 and Al_2O_3 with an average particle size of 12.94 μm. According to the requirements of GB/T 1596-2017, "Fly ash used for cement and concrete", the activity index of fly ash was tested, and its strength activity indexes were 73.6% and 74.6% at 7 days and 28 days, respectively [34–36].

2.2. Experimental Methods

(1) Proportion of desulfurization gypsum-based self-leveling mortar

This experiment aims to prepare desulfurization gypsum based self-leveling mortar so that its performance meets the JC/T 1023-2021, "Gypsum-based self-leveling compound for floor" [37]. Four single-factor experiments were designed to determine the cement content, water-reducing agent, retarder, and methyl hydroxypropyl cellulose ether, and ultimately obtain the mix ratio of desulfurization gypsum–based self–leveling mortar.

(2) Single addition experiment of mineral admixtures

The corresponding steel slag, silica fume, and fly ash were weighed according to 4%, 8%, 12%, 16%, 20%, 24%, 28%, and 32% of desulfurization building gypsum, and separately addedto the desulfurization gypsum–based self–leveling mortar mentioned earlier for flowability and strength testing.

(3) Figure 2 depicts the preparation process of GSLM. Initially, desulfurization building gypsum, cement, mineral admixtures, and admixtures were proportionally weighed. Mineral admixtures and admixtures were added at different percentages of gypsum content, and all measured powders were introduced into the mixer for thorough blending. Proportionally weighed water was poured into the mixing pot, and the uniformly mixed powder was added to the water within a 5-second timeframe. Subsequently, the slurry was mixed for 1 min before being poured into the cement sand mold for molding.

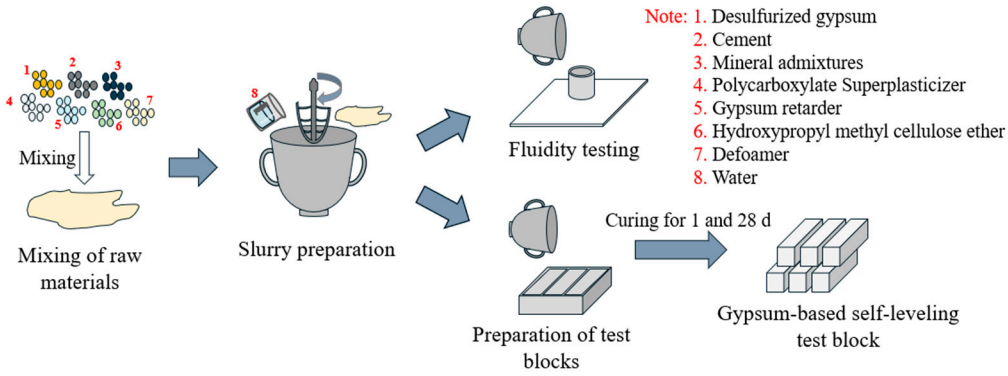


Figure 2. Preparation process of gypsum-based self-leveling mortar.

2.3. Material Characterizations

The fluidity tests were conducted following JC/T 1023-2021, "Gypsum-based self-leveling compound for floor." The fluidity test mold, with a diameter of 30 mm and height of 50 mm, was positioned horizontally at the center of the plate glass. Fresh mortar was then poured into the fluidity test mold, allowing for a 4 min free flow. The initial fluidity was determined by taking the arithmetic mean value of its diameters in both vertical directions. For the 30 min fluidity, the mortar stood for 30 min initially, and its fluidity was measured after 30 s of stirring.

Mechanical strength testing was carried out using a microcomputer-controlled electronic pressure testing machine (DYE-300S, Wuxi Dejiayi Testing Instrument Co., Ltd., Wuxi, China). The loading rates were 0.05 and 2.4 kN/s, respectively, for the flexural and compressive strength. Six specimens, each having dimensions of 40 mm × 40 mm × 160 mm, were prepared for each experiment and demolded after 1 day. Three samples were taken to measure the 1-day strength. After curing for 28 days under standard conditions, the remaining samples were dried in the oven at 40 ± 2 °C for 2 days until a constant mass was achieved. Subsequently, the 28-day absolute dry strengths of the specimens were measured.

An isothermal conduction calorimeter (Calmetrix I-Cal 8000 HPC) was employed to test the hydration heat evolution of pastes after 24 h at 25 °C. X-ray diffraction (XRD,

Bruker D8 Advance, Rheinstetten, Germany) was utilized to study the hydration product of GSLM pastes. The XRD tests were conducted at 40 kV, 30 mA, 4°/min, and a range of 5° to 80° with steps of 0.02°, using a CuKα anode. A Raman spectrometer (Horiba LabRAM HR Evolution, Kyoto, Japan) was used to obtain images of different molecular vibrations emitted and analyze molecular structures. The wavelength of the excitation laser was 514 nm, with a grating of 400 lines/mm, an aperture of 25 µm, an exposure time of 1 s, and 100 exposures. GSLM specimens were coated with gold, and the microstructures were analyzed by scanning electron microscopy (SEM, Zeiss Sigma 300, Oberkochen, Germany). The electron acceleration voltage of the scanning electron microscope is 20 kV.

3. Results and Discussion

3.1. Determination of the Basic Mix Ratio of Flue Gas Desulfurization Gypsum-Based Self-Leveling Mortar

Figure 3 illustrates the flexural and compressive strengths of GSLM samples with varying cement content (the proportion of cement to total cementitious materials). The strengths exhibited an upward trend as the cement content increased. At a cement content of 12%, the flexural and compressive strengths reached their peak values, measuring 7.2 MPa and 27.2 MPa, respectively. This enhancement was attributed to the hydration reactions among the tricalcium silicate, dicalcium silicate, tricalcium aluminate, and tetracalcium aluminoferrite present in Portland cement clinker and water. These reactions led to the formation of C–S–H and needle-shaped ettringite (AFt) with cementitious properties. Consequently, the hydrated calcium silicate and AFt covered the surface of gypsum particles, filling voids in the mortar and creating a denser mortar structure, thereby enhancing the mechanical properties of GSLMs [38–41].

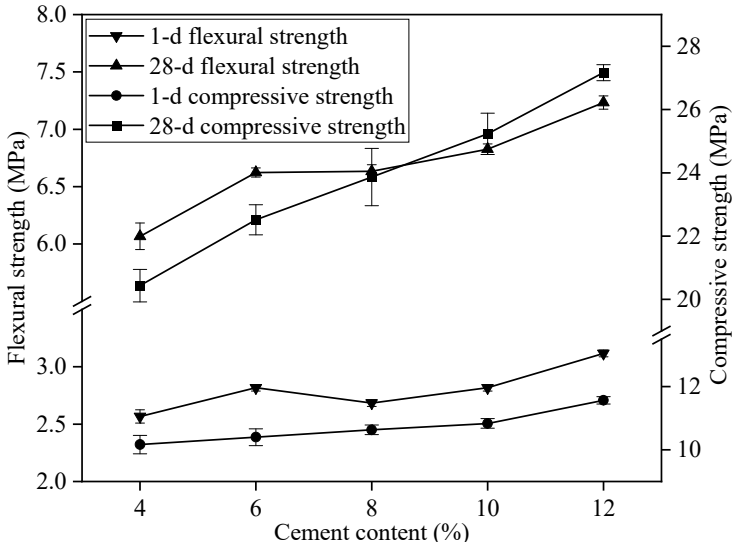


Figure 3. Flexural and compressive strengths of GSLMs with different cement content.

Within the 6% to 8% cement content range, the flexural strength remained constant at 6.6 MPa, while the compressive strength ranged from 22 MPa to 23 MPa. Despite a slight increase in compressive strength, both mechanical properties met the required standards (JC/T 1023-2021: "Gypsum-based self-leveling compound for floor") and the specific values are shown in Table 3. Considering the substantial cost difference between cement and gypsum, it was advisable to minimize the cement content in GSLM formulation based on cost considerations. Consequently, the optimal cement content for subsequent studies was determined to be 6%.

Table 3. Mix proportion and performance of gypsum-based self-leveling materials.

Project	Numerical Value	Requirements in JC/T 1023-2021
Desulfurization building gypsum (%)	94	-
Portland cement (%)	6	-
Polycarboxylate superplasticizer (%)	0.638	-
Polymeric amino acid retarder (%)	0.638	-
Defoamer (%)	0.085	-
HPMC (%)	0.085	-
Water-to-cement ratio	0.54	-
Initial fluidity (mm)	150	-
30 min fluidity (mm)	145	≥140
24-h flexural strength (MPa) strength/MPa	2.8	≥2.0
24-h compressive strength (MPa)	10.5	≥5.0
28-day flexural strength (MPa) strength/MPa	6.6	≥6.0
28-day compressive strength (MPa)	22.5	≥20.0

Figure 4 illustrates the initial fluidity, 30 min fluidity, and fluidity loss of GSLM slurries with various admixtures (calculated additive ratio relative to gypsum). In Figure 4a, the impact of polycarboxylate superplasticizer content on the fluidity of the GSLM slurry was examined. Both initial and 30 min fluidity increased with higher polycarboxylate superplasticizer content, while fluidity loss decreased. Beyond a 0.638% polycarboxylate superplasticizer content, the fluidity of the slurry exhibited minimal change. Therefore, a 0.638% addition of polycarboxylate superplasticizer was deemed optimal.

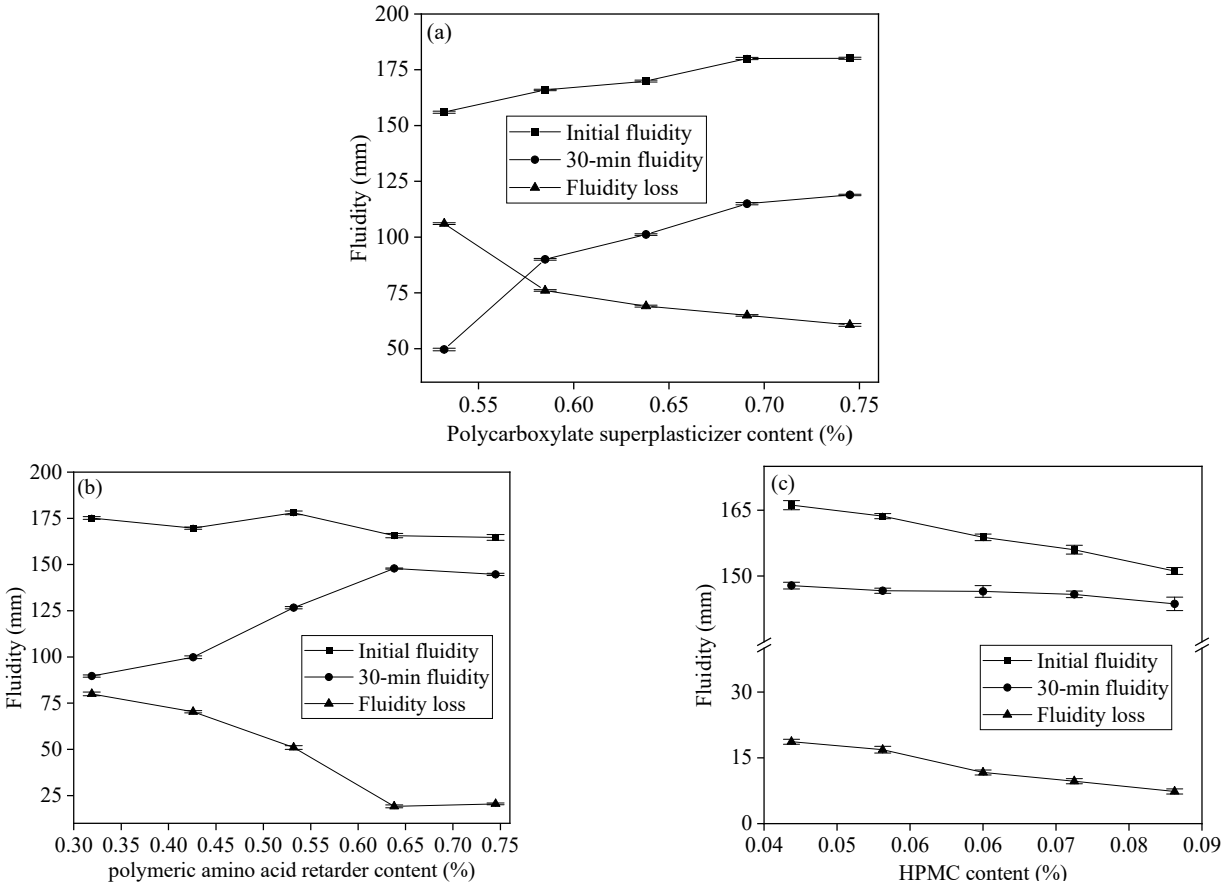


Figure 4. Initial fluidity, 30 min fluidity, and fluidity loss of GSLM slurries with different admixture content. (**a**) Polycarboxylate superplasticizer; (**b**) polymeric amino acid retarder; (**c**) HPMC.

Figure 4b shows that the initial fluidity slightly decreased, 30 min fluidity initially increased and then decreased, and fluidity loss gradually decreased with an increasing content of protein polymeric amino acid retarder. At 0.638% retarder content, the slurry demonstrated an initial fluidity of 167 mm, 30 min fluidity of 148 mm, and fluidity loss of 19 mm. Beyond 0.638% retarder content, the slurry's fluidity showed marginal variations. Hence, 0.638% polymeric amino acid retarder was considered optimal. Furthermore, Figure 4c reveals a significant decrease in slurry fluidity with increasing HPMC content. At 0.085% HPMC content, the initial fluidity essentially met the requirements, falling within the specified range of 145 ± 5 mm (according to JC/T 1023-2021: "Gypsum-based self-leveling compound for floor").

Based on the abovementioned results, the mixing ratios of raw materials, along with the physical and mechanical properties of the GSLM samples, are detailed in Table 3. The fluidity, flexural strength, and compressive strength of the GSLMs all satisfied the standards outlined in the GSLM standard (JC/T 1023-2021).

3.2. Effect of Mineral Admixtures on Physical and Mechanical Properties of Flue Gas Desulfurization Gypsum-Based Self-Leveling Mortar

The impact of SS, SF, and FA content on the initial and 30 min fluidity of the GSLMs is depicted in Figure 5. Both the initial and 30 min fluidity of the GSLMs initially increased and then decreased with rising SS content, as shown in Figure 5a. The 30 min fluidity fell below 140 mm when SS content increased. In Figure 5b,c, the fluidity of the slurry decreases with increasing SF and FA content. Once the content of SF and FA exceeded 16%, the 30 min fluidity of GSLM with SF remained at approximately 139 mm, while that of GSLM with FA exceeded 140 mm. Since SS and FA had particle sizes of 9.34 μm and 12.94 μm, respectively, and SF had a particle size of 1.45 μm, the addition of SS and FA had a comparable effect on initial fluidity of GSLM. However, SF's small particles and high water adsorption capacity diminished slurry fluidity. Moreover, the 30 min fluidity of the slurries exhibited minimal change, as both SF and FA consisted of amorphous spherical particles with a glass microbead effect. Conversely, SS, with its irregular particles, increased frictional forces between particles, resulting in reduced slurry fluidity with higher SS content [24,41].

Figure 6 illustrates the impact of three mineral admixture contents (SS, SF, and FA) on the mechanical properties of GSLMs. Both flexural and compressive strengths of GSLMs initially increased and then decreased with the rising content of SS, SF, and FA. In Figure 6a, the optimal flexural and compressive strengths, at 6.60 MPa and 20.40 MPa, were achieved with 16% SS content. For GSLM with SF (Figure 6b), the highest flexural and compressive strengths, measuring 6.57 MPa and 15.20 MPa, respectively, were observed at 20% SF content. Furthermore, the 1-day flexural and compressive strengths of the GSLMs with FA were approximately 2.30 MPa and 7.80 MPa, respectively (Figure 6c). However, for a 28-day curing period, the highest flexural and compressive strengths were attained with 20% FA content, measuring 8.13 MPa and 16.92 MPa, respectively.

The particles of the three mineral admixtures effectively filled the internal pores of GSLM, enhancing its compactness and leading to a continued increase in flexural and compressive strengths. Nevertheless, when the SS content exceeded 16% or the SF and FA content exceeded 20%, a downward trend in flexural and compressive strengths was observed. This suggests that excessive addition of mineral admixtures may compromise the structure between hydration products. Therefore, the optimal content for SS, SF, and FA in GSLMs was determined to be 16%, 20%, and 20%, respectively.

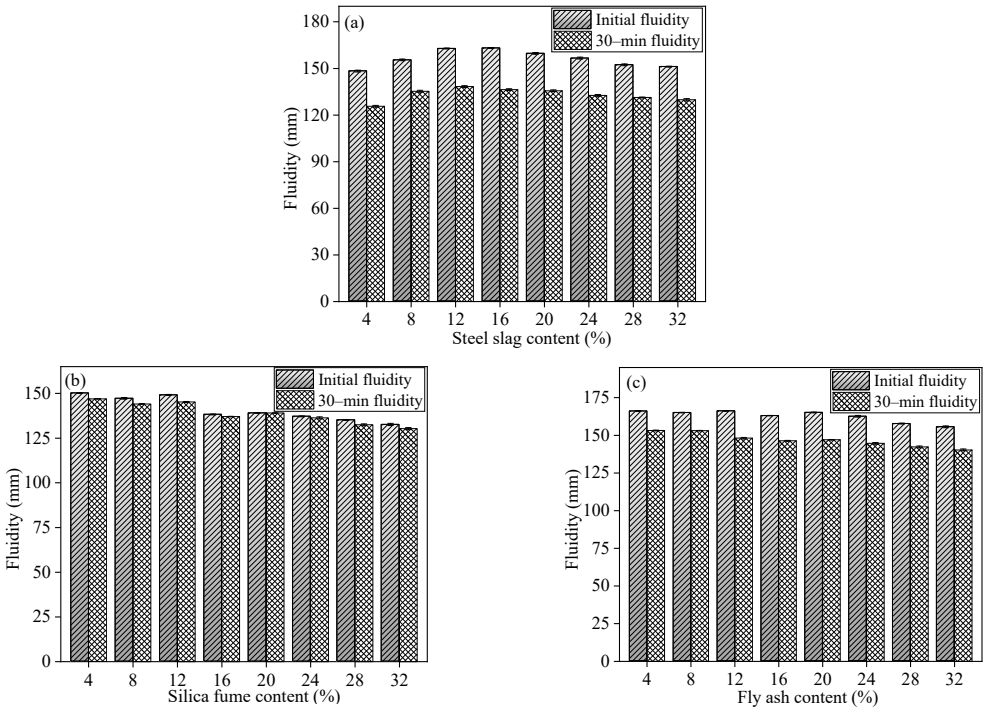


Figure 5. Initial and 30 min fluidity of GSLMs with different steel slag (SS), silica fume (SF), and fly ash (FA) content, respectively. (**a**) GSLM with different SS content; (**b**) GSLM with different SF content; (**c**) GSLM with different FA content.

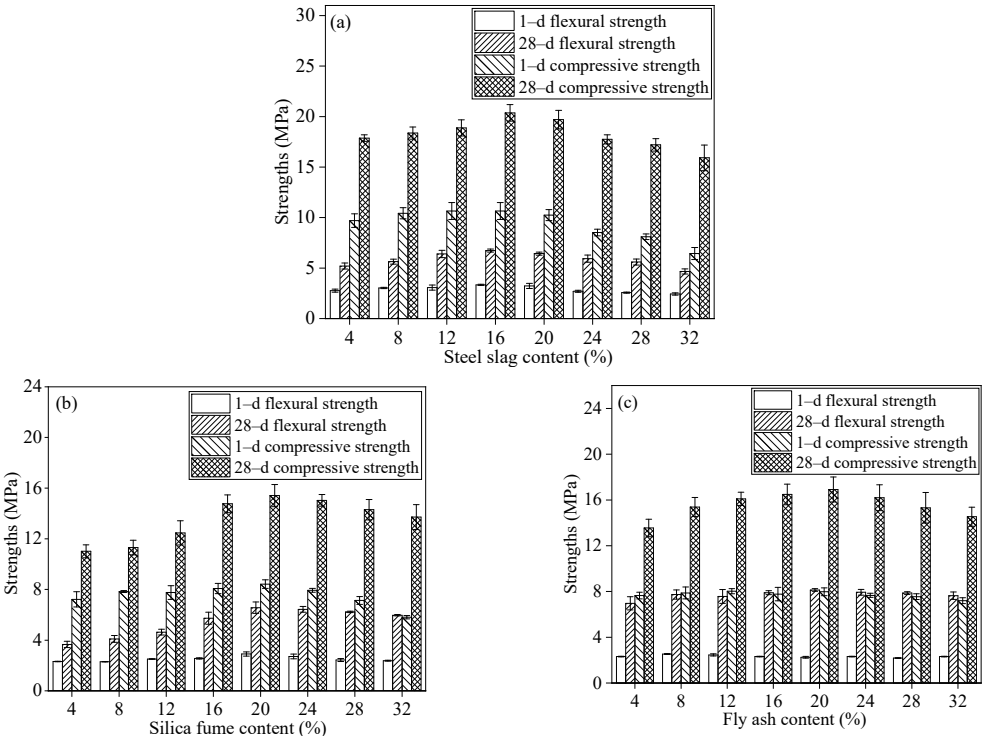


Figure 6. Flexural and compressive strengths of GSLMs with different steel slag (SS), silica fume (SF), and fly ash (FA) content, respectively (**a**) GSLM with different SS content; (**b**) GSLM with different SF content; (**c**) GSLM with different FA content.

3.3. Effect of Mineral Admixtures on Microstructural Properties of Flue Gas Desulfurization Gypsum-Based Self-Leveling Mortar

Figure 7 illustrates the hydration heat release curves of the reference sample (GSLMs without mineral admixtures) and GSLMs with various mineral admixtures. The hydration processes for these samples were categorized into two stages. In the first stage, the hydration exothermic peak emerged at 0–1 h, corresponding to the hydration process of hemihydrate gypsum. The addition of mineral admixtures slightly reduced the intensity of the exothermic peaks by delaying the contact between gypsum and water [41]. However, the smaller particles of SF compared to SS and FA provided more sites for the generation of gypsum hydration products [42]. Consequently, the peak heat release rate of GSLM with SF exceeded that of GSLM with SS and FA. Despite the relatively insignificant difference in particle size between FA and SS, the amount of FA added was slightly higher than that of SS.

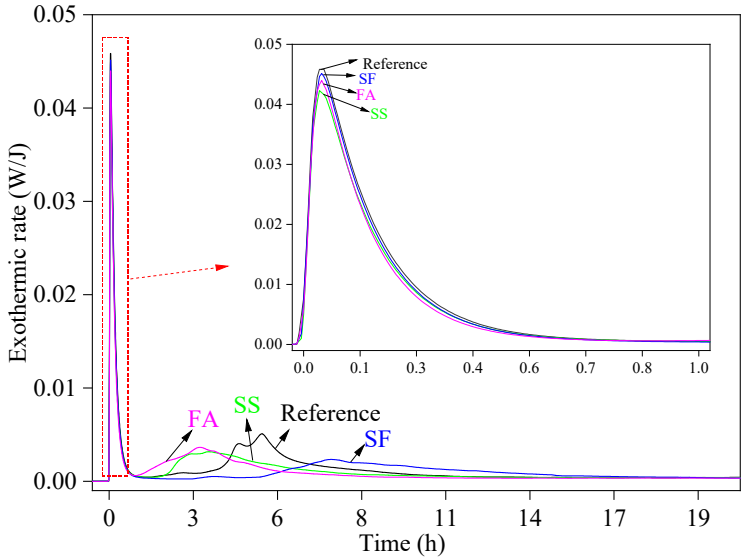


Figure 7. Hydration heat curves of the reference sample and GSLMs with steel slag (SS), silica fume (SF), and fly ash (FA), respectively.

In the second hydration process stage, the hydration exothermic peak appeared between 1 and 16 h, corresponding to the hydration process of ordinary Portland cement (grade 42.5R) and mineral admixtures. The difference in the appearance time of the second hydration heat release peak indicated that the addition of SS and FA accelerated the hydration time, leading to a slight reduction in hydration heat release compared to the reference sample. Conversely, SF delayed the hydration time and significantly reduced heat release during hydration.

Figure 8 displays the XRD patterns of the reference sample and GSLMs with varying SS, SF, and FA content. In Figure 8a, the primary phases for the 1-day and 28-day reference sample were $CaSO_4 \cdot 2H_2O$, C–S–H gel, and AFt. $CaSO_4 \cdot 2H_2O$ resulted from the reaction of $0.5CaSO_4 \cdot 2H_2O$ with water, while C–S–H gel and AFt were products of cement hydration. There was minimal change in the content of these three hydration products between the 1-day and 28-day GSLMs, suggesting that the main hydration reactions were completed within 1 day, consistent with the results of hydration time of the reference sample.

Figure 8b illustrates the main phases—$CaSO_4 \cdot 2H_2O$, C–S–H gel, AFt, RO phase, and Ca_3SiO_5—for the 28-day GSLM with SS. RO phase and Ca_3SiO_5 were present in the raw materials of SS [42–45]. The diffraction intensity of RO phase and Ca_3SiO_5 increased gradually with rising SS content, while the AFt content slightly increased. The AFt content reached its maximum at 16% SS content and remained constant beyond that point. Hence, with 16% SS content, the GSLM exhibited its highest strength, indicating that a portion of SS participated in hydration reactions while the remainder acted as filler.

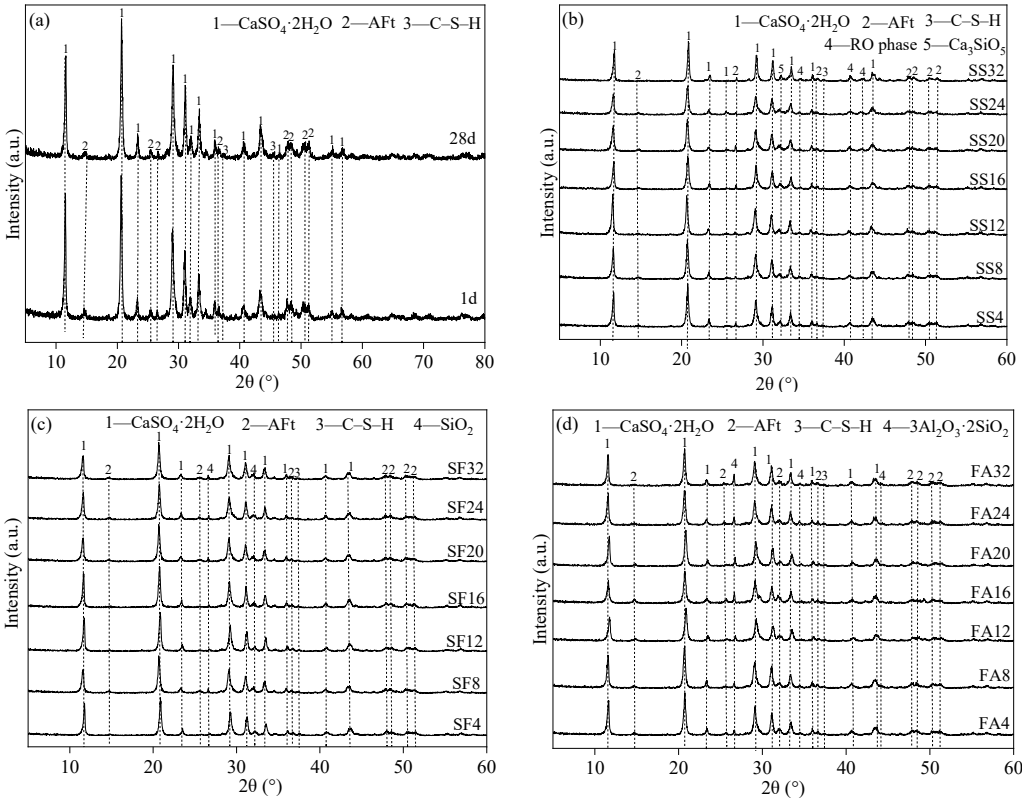


Figure 8. XRD patterns of the reference sample and GSLMs with different steel slag (SS), silica fume (SF), and fly ash (FA) content, respectively. (**a**) Reference sample; (**b**) GSLM with different SS content; (**c**) GSLM with different SF content; (**d**) GSLM with different FA content.

Figure 8c,d shows the main phases: $CaSO_4 \cdot 2H_2O$, C–S–H, AFt, and SiO_2 for GSLM with SF, and $CaSO_4 \cdot 2H_2O$, C–S–H, AFt, and $3Al_2O_3 \cdot 2SiO_2$ for GSLM with FA. With increasing SF and FA content, the diffraction intensity of SiO_2 and $3Al_2O_3 \cdot 2SiO_2$ gradually increased. No new phases were generated during the hydration process, indicating that SF and FA functioned as fillers. The 28-day flexural and compressive strengths of GSLM with SS exceeded those of GSLMs with SF and FA.

Figure 9 illustrates the Raman spectroscopic characterization of the reference sample and GSLMs with 16% SS, 20% SF, and 20% FA, respectively. The characteristic peak at 417 cm^{-1} corresponds to the symmetric bending vibration of $CaSO_4$. The hydration reaction is represented by Equation (1).

$$CaSO_4 \cdot 0.5H_2O + 1.5H_2O \rightarrow CaSO_4 \cdot 2H_2O \quad (1)$$

The distinct characteristic peak at 1017 cm^{-1} originated from the symmetric stretching vibration of [SO_4^{2-}]. In this context, the [SO_4^{2-}] in $CaSO_4$ and AFt overlapped, leading to a higher peak height compared to the other peaks. The hydration reaction of AFt is represented by Equations (2)–(5).

$$C_3A + H_2O \rightarrow C\text{-}A\text{-}H + CH \quad (2)$$

$$C\text{-}A\text{-}H + SO_4^{2-} \rightarrow AFt \quad (3)$$

$$C_3S + H_2O \rightarrow C\text{-}S\text{-}H + CH \quad (4)$$

$$C_2S + H_2O \rightarrow C\text{-}S\text{-}H + CH \quad (5)$$

Here, C–A–H represents calcium aluminate hydrate gel. Additionally, the GSLM containing SS displayed a peak at 490 cm^{-1} attributed to Si–O–Si vibration and a peak at

1085 cm^{-1} arising from the symmetric bending vibration of $[SO_4^{2-}]$ in AFt. These findings indicated that SS reacted with water to form AFt, which was consistent with the XRD results. On the other hand, the curves of GSLM containing SF and FA all exhibited peaks at 490 cm^{-1} due to the tetrahedral vibration of amorphous $[SiO_4]^{4-}$ and 1386 cm^{-1} attributed to amorphous carbon vibration. Furthermore, the curve of GSLM containing FA showed peaks at 760 and 830 cm^{-1}, reflecting tetrahedral vibration of $[SiO_4]^{4-}$. These observations suggest that SF and FA did not participate in hydration, corroborating the XRD results.

Figure 10 illustrates the microstructures of the reference sample and GSLMs with 16% SS, 20% SF, and 20% FA. In Figure 10a–d, the similar pore structures of the specimen section imply that these samples shared pore structures determined by the hydration products of gypsum. Furthermore, in Figure 10a, sheet-like and needle-shaped dihydrate calcium sulfate crystals were interwoven and irregularly distributed. The C–S–H gel produced by cement hydration, along with a small amount of acicular AFt, filled the pores of calcium sulfate dihydrate crystals, contributing to a more compact structure and improved 28-day strength of GSLM.

Figure 10b–d reveal more AFt crystals in GSLM with SS than GSLM with SF and FA, indicating the partial participation of SS in the hydration reaction. Additionally, AFt crystals generated from GSLM with SS were slightly thicker and shorter than those in the reference sample, causing minor damage to the connection between hydration products. Consequently, the 28-day flexural and compressive strengths of GSLM with SS were marginally lower than those of the reference sample. Smooth circular SF and FA particles, filling the pores of hydration products and not participating in hydration reactions, are prevalent in Figure 10c,d. The weak interfaces between the particles and hydration products, owing to the smooth particle surface, made them prone to crack propagation under stress. Therefore, the 28-day flexural and compressive strengths of GSLM with SF and FA were lower, which was consistent with the strength results.

SF and FA, with their regular circular shapes and microbead effect, enhanced GSLM slurry fluidity. In contrast, the irregular shape of steel slag particles increased friction force in the GSLM slurry. Consequently, GSLM slurry with SF and FA experienced less fluidity loss after 30 min, consistent with previous fluidity test results.

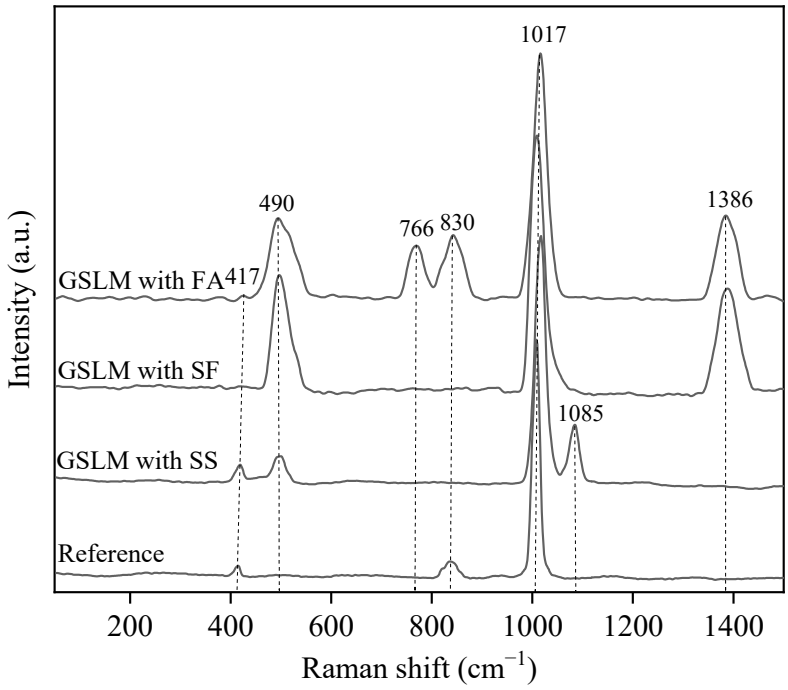


Figure 9. Raman spectroscopy of the reference sample and GSLMs with 16% steel slag, 20% silica fume, and 20% fly ash, respectively.

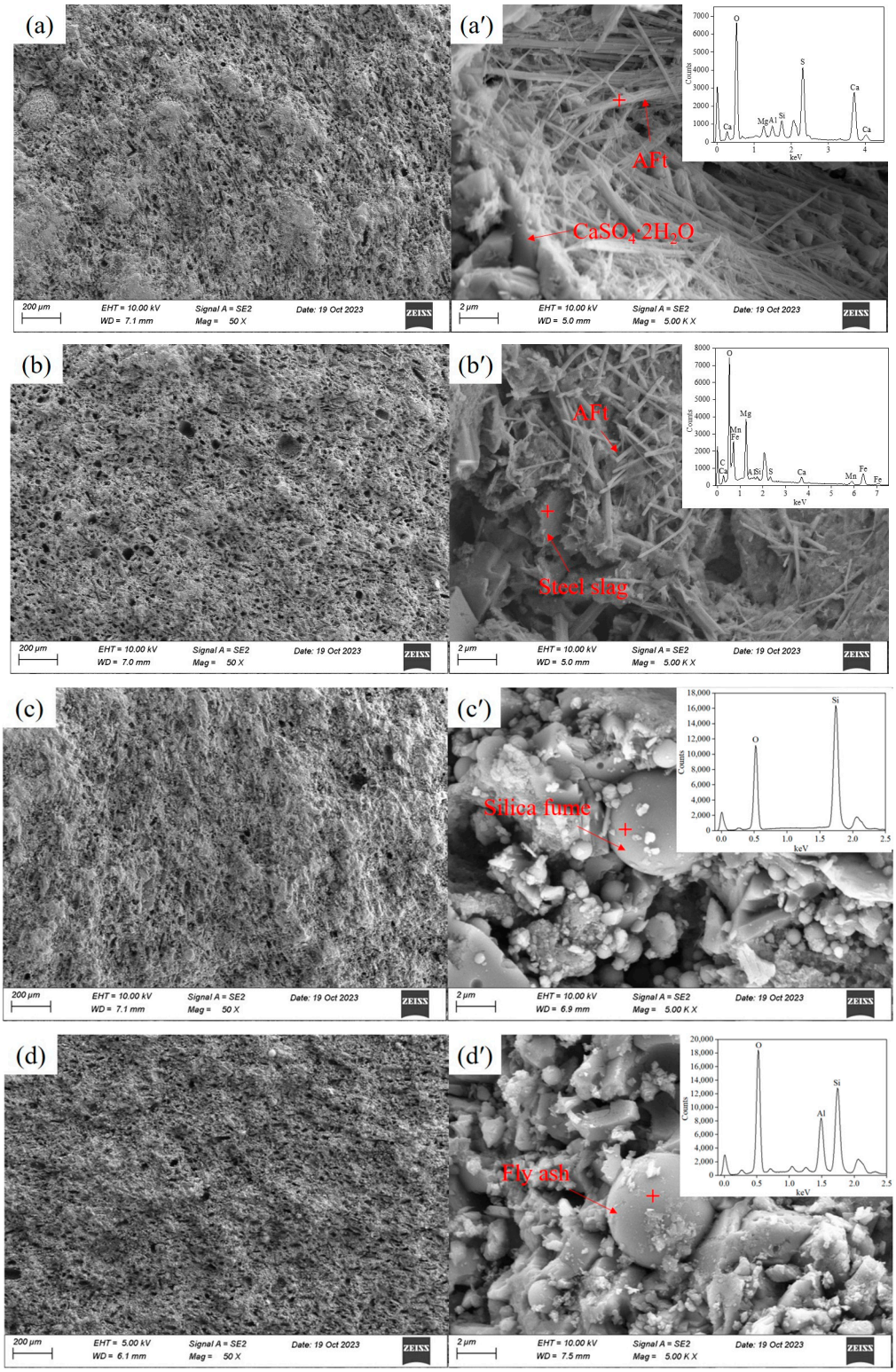


Figure 10. SEM morphology of the reference sample and GSLMs with 16% steel slag, 20% silica fume, and 20% fly ash, respectively. (**a**–**d**) is the cross-section of the reference sample and GSLMs with 16% steel slag, 20% silica fume, and 20% fly ash, respectively, (**a′**–**d′**) is a locally enlarged view of the cross-section of the reference sample and GSLMs with 16% steel slag, 20% silica fume, and 20% fly ash, respectively.

4. Conclusions

(1) The GSLM with SF exhibited the lowest initial fluidity, attributed to the finer particles, larger specific surface area, and higher water absorption capacity of SF particles. However, the smooth spherical nature of SF, with a glass bead effect, had minimal impact on the 30 min fluidity of GSLM.

(2) The strength of GSLM demonstrated an initial increase followed by a decrease with rising SS, SF, and FA content. The mineral admixtures effectively filled internal pores in GSLM, but excessive content could compromise the structure between hydration products. Consequently, the optimal content for SS, SF, and FA in GSLMs is 16%, 20%, and 20%, respectively.

(3) The hydration products of GSLMs with SS, SF, and FA mainly comprised $CaSO_4 \cdot 2H_2O$, C–S–H gel and AFt. A small amount of SS exhibited continued hydration due to the stimulation of calcium hydroxide. The spherical nature of SF and FA, combined with a weak interface with hydration products, facilitated crack propagation from the interface under stress.

(4) In the future, the effects of three-phase composition, particle size of desulfurization building gypsum, and multiple mineral admixtures on the performance of gypsum-based self-leveling mortar should be researched.

Author Contributions: Conceptualization, Y.C. and C.C.; methodology, Y.C. and C.C.; validation, S.W.; formal analysis, C.C. and S.W.; investigation, S.W.; resources, Y.C.; data curation, S.W.; writing—original draft preparation, S.W.; writing—review and editing, Y.C., C.C. and W.Z.; supervision, C.C. and Y.C.; project administration, Y.C. and C.C.; funding acquisition, Y.C. and C.C. All authors have read and agreed to the published version of the manuscript.

Funding: This work was supported by "the 14th Five-Year" National Science and Technology Major Project of China (2022YFC3801401) and the Shaanxi Provincial Innovation Capability Support Program (2021TD-53).

Institutional Review Board Statement: Not applicable.

Informed Consent Statement: Not applicable.

Data Availability Statement: Data are contained within the article.

Conflicts of Interest: The authors declare no conflicts of interest.

References

1. Aakriti; Maiti, S.; Jain, N.; Malik, J. A comprehensive review of flue gas desulphurized gypsum: Production, properties, and applications. *Constr. Build. Mater.* **2023**, *393*, 131918. [CrossRef]
2. Liu, S.; Liu, W.; Jiao, F.; Qin, W.; Yang, C. Production and resource utilization of flue gas desulfurized gypsum in China—A review. *Environ. Pollut.* **2021**, *288*, 117799. [CrossRef]
3. Li, X.; Han, J.; Liu, Y.; Dou, Z.; Zhang, T.-A. Summary of research progress on industrial flue gas desulfurization technology. *Sep. Purif. Technol.* **2022**, *281*, 119849. [CrossRef]
4. Rivero, A.J.; Sathre, R.; Navarro, J.G. Life cycle energy and material flow implications of gypsum plasterboard recycling in the European Union, Resources. *Conserv. Recycl.* **2016**, *108*, 171–181. [CrossRef]
5. Wang, T.; Wu, K.; Wu, M. Development of green binder systems based on flue gas desulfurization gypsum and fly ash incorporating slag or steel slag powders. *Constr. Build. Mater.* **2020**, *265*, 120275. [CrossRef]
6. Geraldo, R.H.; Costa, A.R.; Kanai, J.; Silva, J.S.; Souza, J.D.; Andrade, H.M.; Goncalves, J.P.; Fontanini, P.S.; Camarini, G. Calcination parameters on phosphogypsum waste recycling. *Constr. Build. Mater.* **2020**, *256*, 119406. [CrossRef]
7. Jian, S.; Yang, X.; Gao, W.; Li, B.; Gao, X.; Huang, W.; Tan, H.; Lei, Y. Study on performance and function mechanisms of whisker modified flue gas desulfurization (FGD) gypsum. *Constr. Build. Mater.* **2021**, *301*, 124341. [CrossRef]
8. Lei, D.Y.; Guo, L.P.; Sun, W.; Liu, J.P.; Miao, C.W. Study on properties of untreated FGD gypsum-based high-strength building materials. *Constr. Build. Mater.* **2017**, *153*, 765–773. [CrossRef]
9. Yang, L.; Jing, M.; Lu, L.; Zhu, X.; Zhao, P.; Chen, M.; Li, L.; Liu, J. Effects of modified materials prepared from wastes on the performance of flue gas desulfurization gypsum-based composite wall materials. *Constr. Build. Mater.* **2020**, *257*, 119519. [CrossRef]
10. Xu, L.; Wu, K.; Li, N.; Zhou, X.; Wang, P. Utilization of flue gas desulfurization gypsum for producing calcium sulfoaluminate cement. *J. Clean. Prod.* **2017**, *161*, 803–811. [CrossRef]

11. Wang, X.; Ni, W.; Li, J.; Zhang, S.; Hitch, M.; Pascual, R. Carbonation of steel slag and gypsum for building materials and associated reaction mechanisms. *Cem. Concr. Res.* **2019**, *125*, 105893. [CrossRef]
12. Bartley, P.C.; Erbrick, L.B.; Knotts, M.J.; Watts, D.B.; Torbert, H.A. Influence of Flue Gas Desulfurization Gypsum on Phosphorous Loss in Pine Bark Substrates. *Agriculture* **2023**, *13*, 283. [CrossRef]
13. Yang, J.; Liu, L.; Liao, Q.; Wu, J.; Li, J.; Zhang, L. Effect of superabsorbent polymers on the drying and autogenous shrinkage properties of self-leveling mortar. *Constr. Build. Mater.* **2019**, *201*, 401–407. [CrossRef]
14. Canbaz, M.; Topçu, İ.B.; Ateşin, Ö. Effect of admixture ratio and aggregate type on self-leveling screed properties. *Constr. Build. Mater.* **2016**, *116*, 32l–325. [CrossRef]
15. Anjos, M.A.; Araujo, T.R.; Ferreira, R.L.; Farias, E.C.; Martinelli, A.E. Properties of self—leveling mortars incorporating a high-volume of sugar cane bagasse ash as partial Portland cement replacement. *J. Build. Eng.* **2020**, *32*, 101694. [CrossRef]
16. Zhu, C.; Zhang, J.; Peng, J.; Cao, W.; Liu, J. Physical and mechanical properties of gypsum-based composites reinforced with PVA and PP fibers. *Constr. Build. Mater.* **2018**, *163*, 695–705. [CrossRef]
17. Kondratieva, N.; Barre, M.; Goutenoire, F.; Sanytsky, M. Study of modified gypsum binder. *Constr. Build. Mater.* **2017**, *149*, 535–542. [CrossRef]
18. Wu, H.C.; Xia, Y.M.; Hu, X.Y.; Liu, X. Improvement on mechanical strength and water absorption of gypsum modeling material with synthetic polymers. *Ceram. Int.* **2014**, *40*, 14899–14906. [CrossRef]
19. Nguyen, H.; Adesanya, E.; Ohenoja, K.; Kriskova, L.; Pontikes, Y.; Kinnunen, P.; Illikainen, M. Byproduct-based ettringite binder–a synergy between ladle slag and gypsum. *Constr. Build. Mater.* **2019**, *197*, 143–151. [CrossRef]
20. Liu, C.B.; Gao, J.M.; Tang, Y.B.; Chen, X. Preparation and characterization of gypsum–based materials used for 3D robocasting. *J. Mater. Sci.* **2018**, *53*, 16415–16422. [CrossRef]
21. Zhang, J.; Zhang, Y.; Liu, J.; Miao, Y.; Duan, S. Study on application of gypsum-based self-leveling mortar in floor heating backfill. *Mater. Sci. Eng.* **2020**, *780*, 042010. [CrossRef]
22. Qi, H.; Ma, B.; Tan, H.; Su, Y.; Lu, W.; Jin, Z. Influence of fluoride ion on the performance of PCE in hemihydrate gypsum pastes. *J. Build. Eng.* **2022**, *46*, 103582. [CrossRef]
23. Jin, Z.; Ma, B.; Su, Y.; Lu, W.; Qi, H.; Hu, P. Effect of calcium sulphoaluminate cement on mechanical strength and waterproof properties of beta-hemihydrate phosphogypsum. *Constr. Build. Mater.* **2020**, *242*, 118198. [CrossRef]
24. Jia, R.; Wang, Q.; Luo, T. Reuse of phosphogypsum as hemihydrate gypsum: The negative effect and content control of H_3PO_4. Resources. *Conserv. Recycl.* **2021**, *174*, 105830. [CrossRef]
25. Yang, L.; Zhang, Y.; Yan, Y. Utilization of original phosphogypsum as raw material for the preparation of self-leveling mortar. *J. Clean. Prod.* **2016**, *127*, 204e213. [CrossRef]
26. Zhang, S.; Xu, X.; Memon, S.A.; Dong, Z.; Li, D.; Cui, H. Effect of calcium sulfate type and dosage on properties of calcium aluminate cement-based self-leveling mortar. *Constr. Build. Mater.* **2018**, *167*, 253–262. [CrossRef]
27. Xiao, X.; Li, J.; Meng, Q.; Hou, X.; Liu, Y.; Wang, X.; Wang, W.; Lu, S.; Li, Y.; Mao, Y.; et al. Reuse of by-product gypsum with solid wastes-derived sulfoaluminate cement modification for the preparation of self-leveling mortar and influence mechanism of H_3PO_4. *Constr. Build. Mater.* **2024**, *411*, 134298. [CrossRef]
28. Zhang, J.; Zhang, Y.; Liu, J.; Miao, Y. Study on the Properties of Gypsum-based Self-leveling Mortar using Molybdenum Tailings. *Earth Environ. Sci.* **2019**, *330*, 042002. [CrossRef]
29. Silva, D.B.P.; Lima, N.B.; Estolano, A.; Nascimento, H.; Vilemen, P.; Padron-Hernández, E.; Carneiro, A.; Lima, N.; Povoas, Y. Producing a gypsum-based self-leveling mortar for subfloor modified by polycarboxylate admixture (PCE). *Constr. Build. Mater.* **2023**, *364*, 130007. [CrossRef]
30. Tan, H.; Deng, X.; Gu, B.; Ma, B.; Luo, S.; Zhi, Z.; Guo, Y.; Zou, F. Effect of borax and sodium tripolyphosphate on fluidity of gypsum paste plasticized by polycarboxylate superplasticizer. *Constr. Build. Mater.* **2018**, *176*, 394–402. [CrossRef]
31. Li, Z.; Wang, X.; Hou, Y.; Wu, Z. Optimization of mechanical properties and water absorption behavior of building gypsum by ternary matrix mixture. *Constr. Build. Mater.* **2022**, *350*, 128910. [CrossRef]
32. Gou, M.; Zhao, M.; Zhou, L.; Zhao, J.; Hou, W.; Ma, W.; Hou, Z. Hydration and mechanical properties of FGD gypsum-cement-mineral powder composites. *J. Build. Eng.* **2023**, *69*, 106288. [CrossRef]
33. Zhou, Y.; Xie, L.; Kong, D.; Peng, D.; Zheng, T. Research on optimizing performance of desulfurization-gypsum-based composite cementitious materials based on response surface method. *Constr. Build. Mater.* **2022**, *341*, 127874. [CrossRef]
34. *GB/T 20491-2017*; Steel Slag Powder Used for Cement and Concrete. China Standards Publishing House: Beijing, China, 2017.
35. *GB/T 27690-2023*; Silica Fume for Cement Mortar and Concrete. China Standards Publishing House: Beijing, China, 2023.
36. *GB/T 1596-2017*; Fly Ash Used for Cement and Concrete. China Standards Publishing House: Beijing, China, 2017.
37. *JC/T 1023-2021*; Gypsum Based Self-Leveling Compound for Floor. China Standards Publishing House: Beijing, China, 2021.
38. Wu, Q.; Ma, H.; Chen, Q.; Huang, Z.; Zhang, C.; Yang, T. Preparation of waterproof block by silicate clinker modified FGD gypsum. *Constr. Build. Mater.* **2019**, *214*, 318–325. [CrossRef]
39. Wan, Y.; Hui, X.; He, X.; Li, J.; Xue, J.; Feng, D.; Liu, X.; Wang, S. Performance of green binder developed from flue gas desulfurization gypsum incorporating Portland cement and large-volume fly ash. *Constr. Build. Mater.* **2022**, *348*, 128679. [CrossRef]
40. Magazzù, A.; Marcuello, C. Investigation of Soft Matter Nanomechanics by Atomic Force Microscopy and Optical Tweezers: A Comprehensive Review. *Nanomaterials* **2023**, *13*, 963. [CrossRef]

41. Lesovik, V.; Chernysheva, N.; Fediuk, R.; Amran, M.; Murali, G.; de Azevedo, A.R.G. Optimization of fresh properties and durability of the green gypsum-cement paste. *Constr. Build. Mater.* **2021**, *287*, 123035. [CrossRef]
42. Wang, Q.; Jia, R. A novel gypsum-based self-leveling mortar produced by phosphorus building gypsum. *Constr. Build. Mater.* **2019**, *226*, 11–20. [CrossRef]
43. Chen, M.X.; Li, L.B.; Zheng, Y.; Zhao, P.; Lu, L.; Cheng, X. Rheological and mechanical properties of admixtures modified 3D printing sulphoaluminate cementitious materials. *Constr. Build. Mater.* **2018**, *189*, 601–611. [CrossRef]
44. Liu, Z.; Ni, W.; Li, Y.; Ba, H.; Li, N.; Ju, Y.; Zhao, B.; Jia, G.; Hu, W. The mechanism of hydration reaction of granulated blast furnace slag-steel slag-refining slag-desulfurization gypsum-based clinker-free cementitious materials. *J. Build. Eng.* **2021**, *44*, 103289. [CrossRef]
45. Lu, T.H.; Cchen, Y.L.; Shih, P.H.; Chang, J.E. Use of basic oxygen furnace slag finnes in the production of cementitious mortars and the effects on mortar expansion. *Constr. Build. Mater.* **2018**, *167*, 768–774. [CrossRef]

Disclaimer/Publisher's Note: The statements, opinions and data contained in all publications are solely those of the individual author(s) and contributor(s) and not of MDPI and/or the editor(s). MDPI and/or the editor(s) disclaim responsibility for any injury to people or property resulting from any ideas, methods, instructions or products referred to in the content.